Antioxidant, antibacterial, and cytotoxic activities of cimemoxin derivatives and their molecular docking studies

Velmurugan Loganathan [a], Anis Ahamed [b], Idhayadhulla Akbar [a,*], Saud Alarifi [c], Gurusamy Raman [d]

[a] Research Department of Chemistry, Nehru Memorial College (Affiliated Bharathidasan University), Puthanampatti-621007, Tamil Nadu, India
[b] Department of Botany and Microbiology, College of Science, King Saud University, P.O. Box 2455, Riyadh 11451, Saudi Arabia
[c] Department of Zoology, College of Science, King Saud University, P.O. Box 2455, Riyadh 11451, Saudi Arabia
[d] Department of Life Sciences, Yeungnam University, Gyeongsan 38541, Gyeongsan-buk, South Korea

ABSTRACT

Purpose: The cimemoxin derivatives and their biological importance in antioxidant, antibacterial, and cytotoxic activities were the main focus of this study. By using a one-step reaction and green chemistry method, this study was able to synthesise derivatives of cimemoxin-related Mannich base compounds.
Methods: Green chemistry can be used to prepare new, one-pot syntheses of cimemoxin derivatives (**1a-i**) Mannich base derivatives. FTIR, mass spectrometry, elemental analysis, and ^{1}H and ^{13}C NMR were used to analyse the newly synthesised compounds. The cytotoxic, antibacterial, and antioxidant activities of synthesized compounds (**1a-i**) were investigated. To test all synthesised compounds (**1a–i**) for cytotoxicity against normal Vero cell lines and MCF-7, the antioxidant activities were studied using DPPH, NO, H_2O_2, and ABTS$^{\bullet+}$ assays. The synthesised compounds were screened for anti-tyrosinase and antibacterial activities. Highly active compounds were investigated using molecular docking studies.
Results: The compound **1h** showed considerable activity in H_2O_2 (IC$_{50}$: 13.79 µg/mL) and DPPH-scavenging was significantly active (IC$_{50}$: 19.62 µg/mL) compared to the standard BHT (IC$_{50}$: 27.16 and 33.88 µg/mL). Compound **1f** was more effective than trolox (85.28 %) against ABTS and AAPH antioxidants. The most potent inhibitory activity was observed for compound **1h** (IC$_{50}$ = 15.16 µg/mL) which was more potent than kojic acid (IC$_{50}$ = 17.79 $\pm$ 0.95 µg/mL). All synthetic substances were tested for their cytotoxic potential. Compound **1f** (IC$_{50}$ = 0.12 µg/mL) was extremely active compared to doxorubicin (IC$_{50}$ = 0.74 µg/ml) and other compounds were lowly active compared to the MCF-7 cell line. In terms of anti-tyrosinase activity, compound **1h** was highly active compared with the standard, and compound **1d** was highly active against *K. pneumonia*.
Conclusion: In this study, strong antioxidant, antibacterial, and cytotoxic activities were reported for all the compounds. In molecular docking studies, compounds **1d** and **1h** had higher binding affinities than the other compounds. Compounds **1d** and **1h** performed well in all tests. Additionally, this investigation successfully identified a number of intriguing compounds with cytotoxic and antioxidant properties.

1. Introduction

Cyclohexane-1,3-dione (1,3-CHD) is the most important molecule used in various industrial applications such as insecticides, polymer additives, and cosmetics (Caine et al., 2020; Caine et al., 2019; Chen et al., 2016). Generally, various methods are used to synthesise cyclohexane-1,3-dione derivatives; for example, the aldol-condensation technique is a very basic condensing agent (Wei et al., 2018), whereas

other alternative methods involve the selective hydrogenation of resorcinol (RES) (Hou et al., 2014). In 1986, Etter et al. published a paper on the crystal structure of 1,3-cyclohexanedione and documented the formation of CHD and benzene inclusion compounds (Etter et al., 1986). A class of chemical compounds known as hydrazine derivatives contain molecules with a functional group —C=N—N=C—. With this conjugated system, electrical stimulation of the near-UV and visible spectra is conceivable. These are important for a variety of applications,

including DSSC (dye-sensitised solar cells) (Sun et al., 2015; Gong et al., 2017), analytical fluorescent sensors for detection (Jung et al., 2019), organ gels, and protection against corrosion (El Azzouzi et al., 2016; Belghiti et al., 2019). Furthermore, the antioxidant, antimicrobial, and anticancer properties of phenyl-substituted hydrazines have been reported (Markova et al., 2019). Despite being utilised as precursors in organic synthesis, derivatives of hydrazine are commonly utilised in the polymer, agricultural, medicinal, and dye industries (Tanini and Capperucci, 2021). It has been discovered that a number of compounds with a hydrazine moiety are efficient in therapy for hypertension, Parkinson's disease, and tuberculosis (TB). Several hydrazine derivatives exhibit substantial biological activities (Popiołek, 2017). Certain hydrazines also exhibit neuroprotective properties and are prescribed as antidepressants (Pan et al., 2021). Azapeptides, which are hydrazine-based peptidomimetics, have been discovered as effective treatments for hepatitis, AIDS, and SARS (Aggarwal et al., 2013). Fig. 1 illustrates that some pesticidal and herbicidal active compounds have 1,3-CHD as their basic unit (a) (Sharma et al., 2021) and a bioactive synthetic hydrazine moiety (b) (Al-Zharani et al., 2022).

Based on these observations, cyclohexane-1,3-dione and hydrazine play significant roles in various industrial and biological fields. In this study, we developed a three-component, one-pot synthesis of 1,3-cyclohexanedione that connects hydrazine derivatives to produce Mannich base cimemoxin derivatives, and evaluated their cytotoxic, antibacterial, anti-tyrosinase, and antioxidant properties. The cytotoxic effects of

Mannich-based cimemoxin derivatives have also been investigated against normal Vero cancer cell lines.

2. Material and methods

2.1. Chemistry

Transparent capillary tubes were used to measure breaking points. FT-IR bands (using Shimadzu 8201 PC, 4000–400 cm^{-1}) were captured in KBr. A Bruker Drx 300WB spectrometer (operating at 300 and 75 MHz) was used to analyse the NMR spectra of all compounds. The mass spectrum (EI) at 70 eV was recorded using a D-300 Jeol JMS mass spectrometer. C, H, N, and S were assessed using an elemental analyser (Vario EL III). TLC was used to determine the purities of the compounds.

2.1.1. Synthesis of compound (1a-1i)

Compound **1a**, 3-methylbut-2-en-1-ylidene hydrazine (0.1 mmol), benzaldehyde (0.1 mmol), and 1,3-cyclohexanedione (0.1 mmol) were added in ethanol. The reaction mixture was refluxed for five hr at 60°C. Before adding the reaction mixture to frozen water, it was stirred and cooled to ambient temperature. The final product was identified and confirmed by thin-layer chromatography (TLC). The solid substance was separated by column chromatography (CC) with ethyl acetate and hexane (4:3 ratio) (Mostafa et al., 2019; Al-Khattaf et al., 2021). The final product was recrystallised using the appropriate alcohols. A yield

(i) Sulcotrione

(ii) Tembotrione

(iii) Tefuryltrione

(i) Larvidial activity (43.06%)
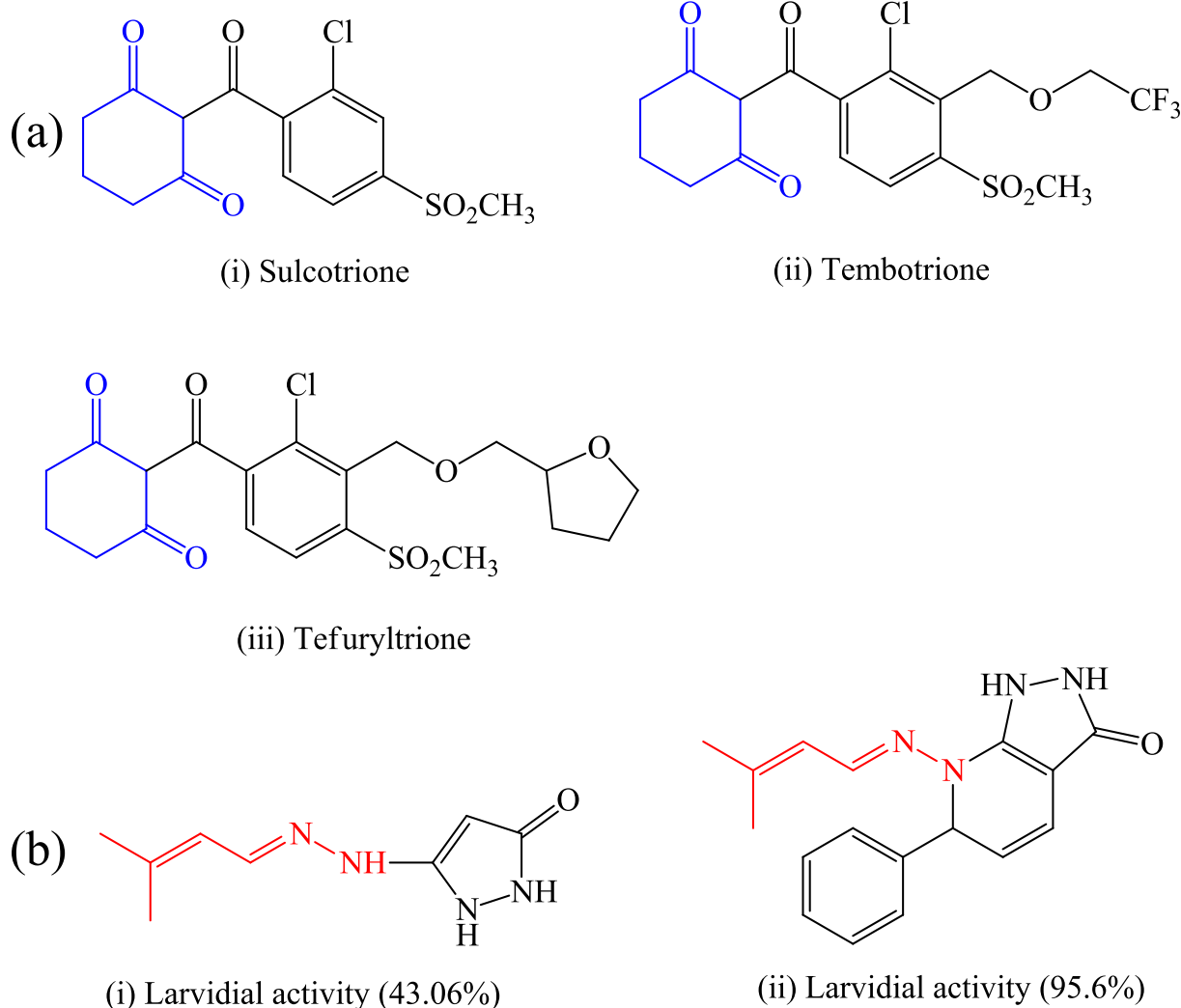
(ii) Larvidial activity (95.6%)

Fig. 1. (a)Herbicidal and pesticidal active componunds having cyclohexane-1,3-dione as basic unit and (b)some bioactive synthetic hydrazine moitey.

of compounds 1(a-i), approximately 78–86 % were obtained. A similar procedure was performed using the remaining compounds (**1b–1i**).

2.2. Antioxidant activity

2.2.1. DPPH scavenging activity

Using the DPPH (2,2-diphenyl-1-picrylhydrazyl) technique of each compound's antioxidant activity was assessed. The antioxidant capabilities of different chemical dosages (10, 25, 50, and 100 µg/mL) were studied. When DPPH was dissolved in methanol, several compounds were examined to determine whether they could protect DPPH from bleaching. At room temperature, 1.6 mL the test sample was combined with a DPPH methanol solution to measure the absorbance and compare it with a control (Surendra Kumar et al., 2017).

The formula was used to determine the % inhibition.

$$DPPHScavengingeffect(\%) = \frac{A_{control} - A_{sample}}{A_{control}} \times 100$$

2.2.2. Hydrogen peroxide (H₂O₂) scavenging assay

Each material was examined for its capacity to scavenge H_2O_2. A solution of H_2O_2 (40 mM) was prepared in a phosphate buffer (pH 7.4). Phosphate buffer (0.6 mL, 40 mM) was dissolved in the test compounds (3.4 mL) (10, 25, 50, and 100 µg/mL) before being added to the H_2O_2 solution. The absorbance of the reaction mixture was examined at 230 nm (Lateef et al., 2017).

H_2O_2 scavenging inhibition was calculated as a percentage.

$$\%ofInhibition = \frac{A_{control} - A_{sample}}{A_{control}} \times 100$$

2.2.3. NO (Nitric oxide) scavenging activity

The NO-scavenging capability of the compounds was assessed. Sodium nitroprusside (10 mM), PBS (0.2 M, pH 7.4), and various quantities of the test sample (10–100 µg/mL) were added throughout the 150-minute incubation at 25 °C. Afterwards, the reaction product (1 mL) was added, followed by Griess reagent (1 mL) (Ghosh and Tiwari, 2018).

H_2O_2 scavenging inhibition was calculated as a percentage.

$$\%ofNOScavanging = \frac{A_{control} - A_{sample}}{A_{control}} \times 100$$

2.2.4. 2,2-azino-bis-3-ethylbenzothiazoline-6-sulphonic acid radical cation (ABTS•⁺) decolorization assay TEAC stands for trolox equivalent antioxidant capacity

These substances were evaluated for their ability to scavenge ABTS•⁺. During the course of 12 h in the dark at ambient temperature, ABTS•⁺ interacted with 2.45 mM $K_2S_2O_8$ to produce ABTS•⁺.

The ABTS•⁺ solution was treated with phosphate buffer until the absorbance at 734 nm (0.1 M, pH 7.4) was 0.700 ± 0.025.

The diluted solution was then given 1.5-mL aliquots of compounds (**1a–i**) at various concentrations (10, 25, 50, and 100 µg/mL). Each concentration was compared to a blank sample (ethanol) after 30 min and the inhibition % was calculated (Alaklabi et al., 2018).

The ABTS•⁺ radical's scavenging efficiency was determined using the following equation:

$$ABTS \cdot + scavengingeffect(\%) = \frac{A_c - A_s}{A_c} \times 100\%$$

2.2.5. Lipid peroxidation method (AAPH)

Linoleic acid peroxidation was investigated for all synthesised substances. To synthesise conjugated diene hydroperoxide, 2,2′-azobis (2-amidinopropane) dihydrochloride (AAPH) was utilised as a free radical accelerator to oxidise a water-based dispersion of linoleic acid at 234 nm. This study may be used to follow oxidative modifications and to measure the effectiveness of each drug in suppressing linoleic acid peroxidation.

A UV cuvette containing phosphate buffer (1 mL of 0.05 M) was tested. AAPH oxidises an aqueous linoleic acid dispersion at 234 nm to form conjugated diene hydroperoxide, a free radical initiator.

This study can be used to monitor oxidative processes and establish the degree to which each medication suppresses linoleic acid peroxidation. The UV cuvette was filled with phosphate buffer (1 mL) and linoleic acid (1 mL) dispersion and warmed to 37 °C. The oxidation process was initiated with 1 mL of the AAPH solution at 37 °C in air. Oxidation was conducted using 1 mL of the examined compounds (10, 25, 50, and 100 µg/mL). A same-volume of DMSO was used to study lipid oxidation with and without antioxidants. The absorbance was measured at 37 °C to assess the oxidation rate (Alaklabi et al., 2018).

Formula for linoleic acid oxidation inhibition:

$$\%Inhibition = \frac{1 - rateofabsorbancechangewithtestcompound}{rateofabsorbancechangewithsolventcontrol} \times 100$$

2.3. Anti-tyrosinase screening

Mushroom tyrosinase activity was evaluated using a modified spectrophotometric technique with L-dopa as the reagent. The mixture for the reaction, which included mushroom tyrosinase (12.428 U), L-DOPA (1.5 mM), sodium phosphate solution (pH 6.5) (0.1 mM), and a final volume (3.0 mL), was incubated at 30 °C for two minutes. Using a UV-160A Shimadzu spectrometer, it was possible to spectrophotometrically measure the production of dopachrome by measuring the absorbance at 475 nm. Kojic acid is a beneficial compound (Selvaraj et al., 2020).

The formula below was used to calculate the percentage of tyrosinase activity inhibition:

$$Tyrosinaseinhibitoryactivity(\%) = \frac{(A - B) - (C - D)}{(A - B)} \times 100$$

Where,

A is after incubation, the neutral solution's absorption; B is before incubation, the neutral solution's absorption; C is the sample solution's color following fermentation; and D is the sample solution's color before processing.

2.4. Cytotoxic screening

The same methods used in an earlier study were used to examine the cytotoxicity of the newly synthesised compounds (**1a–i**). The Supporting Information section provides a full description of the procedure (Surendra Kumar et al., 2017).

2.4.1. Cell lines and cell culture

ATCC provided the MCF-7 and normal Vero cell lines. At 37 °C and 5 % CO_2, DMEM with 10 % FBS was used to cultivate the cells until they achieved 70–80 % confluence.

2.5. In vitro antibacterial screening

A previously described method was used to test the antibacterial activity of the synthesised compounds (**1a–i**). The Supporting information section has a full description of the procedure (Surendra Kumar et al., 2017).

2.6. Molecular docking

2.6.1. Ligand preparation

ChemDraw 12.0 and Chem3Dpro were used to Draw the ligands (Compound **1a-i**); and Protein Data Bank was created from the ligand molecules for docking research (www.cambridgesoft.com).

2.6.2. Receptor preparation

The protein data bank was used to download the structure (PDB ID:

2Y9X and **6B1P**) from http://www.rcsb.org representing a protein-binding mushroom tyrosinase and glutamate-tRNA synthetase. Water molecules and ligands were removed from the Discovery Studio 2019. The energy of the receptor was reduced using SWISS PDB Viewer, after which molecular docking at the receptor was performed.

2.6.3. Identification of the binding pocket

Using a co-crystallised ligand and the Discovery Studio 2019 application, the binding pocket of the target protein was specifically located; 2Y9X - Asp312, Glu356, Lys379, Gln307, Asp357, Trp358, Lys379, and 6B1P – Arg80, Arg157, Arg175, Ile172, Tyr182, Asn183, Lys210 were residues found in the binding pocket.

2.6.4. Docking

Using Auto Dock Vina 1.1.2 (http://mgltools.scripps.edu), molecular docking investigations, to ascertain the interactions and mechanisms between the most potent compounds in the Cimemoxin series, compounds **1d, 1f,** and **1h** with the proteins 2Y9X and 6B1P (Chidambaram et al., 2021).

3. Result and discussion

3.1. Chemistry

Mannich base derivatives have been synthesised using green chemistry. A mixture of 3-methylbut-2-en-1-ylidene hydrazine, benzaldehyde, and 1,3-cyclohexanedione was combined with ethanol and refluxed for 5 h at 60 °C. The final product was identified and confirmed by thin-layer chromatography. The solid substance was separated by column chromatography with ethyl acetate and hexane (4:3 ratio). The resultant solid was recrystallised from a suitable alcohol to produce a pure product. The synthetic route to the cimemoxin derivative is shown in Scheme 1. The product yield was 86–78 %.

The target compounds were analysed using FT-IR and NMR spectroscopy (^1H and ^{13}C). The fundamental classification of the compounds revealed substantial bands in the IR spectrum at 3395–3315, 1815–1680, and 1685–1644 cm^{-1}, adhering to the —NH, CO, and CN groups. ^1H NMR signals showed that δ 7.92–6.90, 7.50, 7.0, 2.16–1.94, and 2.40–2.30 ppm, indicating —Ph, N=CH, —NH, —CH$_3$, and —CH$_2$ protons. The ^{13}C NMR revealed peaks at δ 208.3, 158.6–115.0, 137.2, 40.8, and 20.5–26.9 ppm, which conformed to the CO, —Ph, N=CH, —CH$_2$—, and —CH$_3$ atoms. The results from the elemental analysis and mass spectroscopy agreed with the structure of each compound. The molecular weight was determined by mass spectral characterisation (EI-MS), and **1a** compound shows a molecular ion EI-MS (m/z) of 298.38 (M$^+$, 20.5 %), which was confirmed by the molecular weight of compound **1a**. All compounds conformed to the molecular mass using EI-MS mass spectral analysis. The detailed ^1H and ^{13}C NMR spectra are included in the Supporting Information file (Figs. S1–S18).

Compounds (**1a–i**) were evaluated for their antioxidant activity using UV–visible spectrophotometry and DPPH, H$_2$O$_2$, NO, ABTS$^{•+}$, and AAPH assays. The cytotoxic potential of compounds **1(a–i)** against cancer cell lines (MCF-7 and Vero) was examined. Compounds **1(a-i)** were screened for antibacterial and anti-tyrosinase activities.

3.2. Antioxidant activity

The synthesised compounds **1(a-i)** were screened for antioxidant activity. The ability of compound **1h** to scavenge DPPH free radicals increased with increasing concentration, achieving a maximal activity of 100 % at 100 μg/mL. Compared to conventional BHT (IC$_{50}$ = 33.8 μg/mL), compound 1 h had significantly higher scavenging activity (IC$_{50}$ = 19.62 μg/mL). The other compounds were less active than BHT and compound **1h**. Table 1 shows the DPPH scavenging activity of compound **1(a-i)**. The detailed DPPH scavenging activity values shows in Supporting Information (Table S1).

Cimemoxin derivatives (**1a-i**) has an H$_2$O$_2$ scavenging activity of 10–100 μg/mL. Compounds **1h** (IC$_{50}$ = 13.79 μg/mL) had extraordinary activity (100 μg/mL at 100 % activity) when compared with BHT (IC$_{50}$ = 27.16 μg/mL) and was lower than that of the other compounds had lowly active. The scavenging activities of the compounds against hydrogen peroxide (H$_2$O$_2$) is shown in Table 1. The detailed H$_2$O$_2$ scavenging activity values shows in Supporting Information (Table S2).

Spectrophotometric measurements of formazan, which was formed when the NO radical met the Griess reagent, were performed on all the chemicals that were made. Compounds **1c** (IC$_{50}$ = 23.58 μg/mL) have a high level of activity against both standard BHT (IC$_{50}$ = 31.73 μg/mL) and other substances (80 % activity at 100 μg/mL). Although the most

Table 1
DPPH, H$_2$O$_2$, NO scavenging activity of compounds (**1a-1i**) IC$_{50}$ Value (μg/mL).

Compounds	DPPH scavenging activity	H$_2$O$_2$ scavenging activity	NO scavenging activity
	IC$_{50}$ (μg/mL)	IC$_{50}$ (μg/mL)	IC$_{50}$ (μg/mL)
1a	42.57	44.19	83.44
1b	33.18	20.47	34.23
1c	83.86	47.02	23.58
1d	76.48	47.42	48.00
1e	43.97	82.26	49.02
1f	33.49	40.85	45.39
1g	>100	>100	>100
1h	19.62	13.79	67.82
1i	38.22	>100	>100
BHT	33.88	27.16	31.73

^{a}Value expressed are means ± SD of three different experiments.
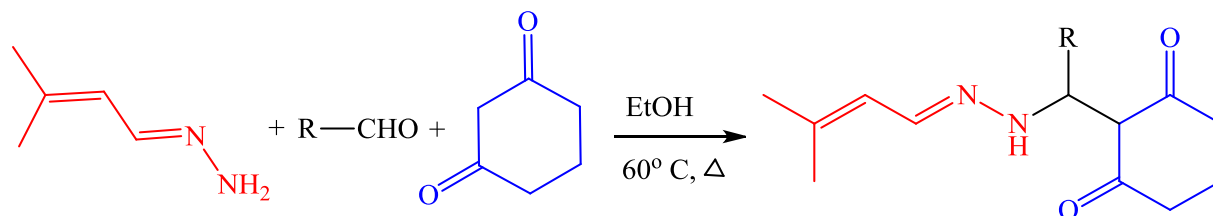
1(a); R = -Ph,   1(b); R = -Ph-Cl,   1(c); R = -Ph-Br,   1(d); R = -Ph-NO$_2$,   1(e); R = -Ph-CH$_3$,

1(f); R= -Ph-OCH$_3$,   1(g); R = -Ph-NH$_2$,   1(h); R = -Ph-OH,   1(i); R = -Ph-F

Scheme 1. Synthesis route of Cimemoxin dervaties.

frequent compounds were very active, compound **1c** was the most active, as shown in Table 1. The detailed NO scavenging activity values shows in Supporting Information (Table S3).

For the ABTS$^{\bullet+}$ assay, cimemoxin derivatives **(1a–i)** was examined. Comparing compound **1f** to trolox (85.28 ± 0.97 %), compound **1f** was much more active (99.08 ± 0.02 %). About 90 % greater activity was displayed by compounds **1e, 1f, 1g, 1h** and **1i** than by Trolox. Table 2 displays the ABTS scavenging activities of the extracts.

The ABTS radical cation, which depends on decolourisation, rapidly generates a stable green/blue ABTS$^{\bullet+}$ prior to its reaction. All compounds had a purity between 80 and 99 % and were more active than normal trolox.

Using the AAPH assay, compounds **(1a–i)** were tested for conjugated diene hydroperoxides. This was done by oxidising linoleic acid at a wavelength of 234 nm, which caused conjugated diene hydroperoxides to be formed by the hydrophilic AAPH initiator. The antioxidant activities of the synthesised compounds were measured. Compound 1f showed the highest antioxidant activity at 97.30 ± 0.10 % at 100 µg/mL (Mani et al., 2021).

3.3. Tyrosinase inhibitory activity

According to Mani et al. (2021), in order to evaluate tyrosinase inhibition, all the synthesised cimemoxin derivatives **(1a-i)** were tested using the substrate L-DOPA, using a slightly modified version of Bradford's technique. Kojic acid was chosen as the standard compound because of its strong inhibitory action against tyrosinase, making it a popular skin-whitening ingredient. The most potent inhibitory activity was observed for compound **1h** (IC$_{50}$ = 15.16 µg/mL) which had highly activity than kojic acid (IC$_{50}$ = 17.79 ± 0.95 µg/mL), and other compounds had lowly active than compound **1h** and standard. Table 3 summarises these activities.

3.4. Cytotoxic activity

The cytotoxic activities of the newly prepared compounds **1(a–i)** were examined according to a previously reported method (Gobinath et al., 2021). Compound **1f** (IC$_{50}$: 0.12 ± 0.04 µg/mL) was much more hazardous than doxorubicin (IC$_{50}$: 0.74–±0.01 µg/mL), because these actions were only seen at quantities higher than 16.16 µg/mL, which is the dose that is 100 % harmful to Vero cell lines. As a result, the compounds **1f** were shown to be cytotoxic for Vero cell lines and to be very active against antioxidant and antibacterial activities. The other compounds were less active than doxorubicin and **1f** (Table 4).

3.5. In vitro antibacterial activity

Synthesised compounds **1(a-i)** were screened for antibacterial activity, compound **1d**, and **1f** (MIC = 2 µg/mL) was highly active against *S. aureus* compared with standard ciprofloxacin, while **1b, 1c, 1e,** and **1**

Table 2
ABTS$^{\bullet+}$ and AAPH activities of compounds (**1a-1i**).

Compounds	Percentage of activity (%)[a]	
	ABTS$^{\bullet+}$	AAPH
1a	80.10 ± 0.02	79.20 ± 0.01
1b	82.19 ± 0.10	82.11 ± 0.31
1c	78.03 ± 0.12	86.20 ± 0.14
1d	80.32 ± 0.50	80.24 ± 0.12
1e	92.18 ± 0.01	92.12 ± 0.01
1f	99.08 ± 0.02	97.30 ± 0.10
1g	93.05 ± 0.03	94.02 ± 0.42
1h	92.32 ± 0.36	92.01 ± 0.04
1i	93.50 ± 0.01	90.33 ± 0.05
Trolox	85.28 ± 0.97	62.39 ± 0.35

[a] Value expressed are means ± SD of three different experiments.

Table 3
Antityrosinase activity of the compounds (**1a-1i**).

Compounds	Concentration(µg/mL)[a]				IC$_{50}$(µg/mL)
	10 µg/mL	25 µg/mL	50 µg/mL	100 µg/mL	
1a	22.13 ± 0.13	35.02 ± 0.03	45.01 ± 0.06	54.13 ± 0.14	79.61
1b	29.17 ± 0.13	42.10 ± 0.31	52.50 ± 0.02	66.15 ± 0.04	52.78
1c	18.60 ± 0.03	26.13 ± 0.16	48.20 ± 0.14	57.12 ± 0.24	75.08
1d	26.14 ± 0.11	44.10 ± 0.65	66.10 ± 0.12	88.23 ± 0.04	37.01
1e	16.10 ± 0.17	24.81 ± 0.26	42.16 ± 0.46	53.19 ± 0.12	85.27
1f	29.04 ± 0.16	48.69 ± 0.11	54.19 ± 0.16	72.13 ± 0.02	43.88
1g	13.05 ± 0.28	27.10 ± 0.12	40.10 ± 0.07	65.10 ± 0.03	70.77
1h	34.04 ± 0.11	64.20 ± 0.65	84.10 ± 0.19	100 ± 0.00	15.16
1i	16.09 ± 0.18	27.10 ± 0.19	43.02 ± 0.03	59.09 ± 0.14	75.55
Kojic acid	42.38 ± 0.02	55.69 ± 0.22	68.18 ± 0.49	84.79 ± 0.36	17.79

[a] Value were the means of three replicates ± SD, -; No active.

Table 4
Cytotoxicity activity of compounds (**1a-i**).

Compounds	MCF-7 cell line			Vero	SI[b]
	GI$_{50}$ (µg/mL)[a]	TGI (µg/mL)[a]	LC$_{50}$ (µg/mL)[a]	LC$_{50}$ (µg/mL)[a]	
1a	10.05 ± 0.01	23.12 ± 0.09	44.10 ± 0.02	46.02 ± 0.01	1.49
1b	19.11 ± 0.14	36.92 ± 0.13	52.10 ± 0.01	57.10 ± 0.12	1.06
1c	26.42 ± 0.13	48.90 ± 0.42	58.00 ± 0.11	65.10 ± 0.05	1.05
1d	24.10 ± 0.50	42.10 ± 0.32	53.01 ± 0.17	29.10 ± 0.08	1.08
1e	0.01 ± 0.00	0.09 ± 0.01	0.40 ± 0.01	12.13 ± 0.06	55.62
1f	0.01 ± 0.00	0.06 ± 0.07	0.12 ± 0.04	16.16 ± 0.51	42.92
1g	0.02 ± 0.00	0.42 ± 0.04	0.69 ± 0.06	22.61 ± 0.70	61.62
1h	0.22 ± 0.01	0.36 ± 0.01	1.69 ± 0.05	19.96 ± 1.71	29.41
1i	1.19 ± 0.26	3.05 ± 0.02	7.16 ± 0.17	36.02 ± 0.05	8.87
Doxorubicin	0.02 ± 0.00	0.21 ± 0.01	0.74 ± 0.01	20.15 ± 0.82	54.62

[a] Data represent the mean ± standard error of the mean values of three separate experiments.
[b] SI = Selectivity Index = IC$_{50}$ value normal cell/IC$_{50}$ value cancer cell.

h (MIC = 4 µg/mL) was equipotent activity compared with standard (MIC = 4 µg/mL). Compound **1d** (MIC = 2 and 1 µg/mL) was highly active against *E. coli* and *P. aeruginosa*, and **1g** and **1i** (MIC = 4 and 2 µg/mL) showed equipotent activity compared with the standard ciprofloxacin. Compound **1d** (MIC = 0.5 µg/mL) was more active against *K. pneumoniae* than ciprofloxacin (MIC = 16 µg/mL) and other compounds. Table 5 shows the antibacterial activities of compounds **1a-i** using MIC (Al-Khattaf et al., 2021).

3.6. Molecular docking studies

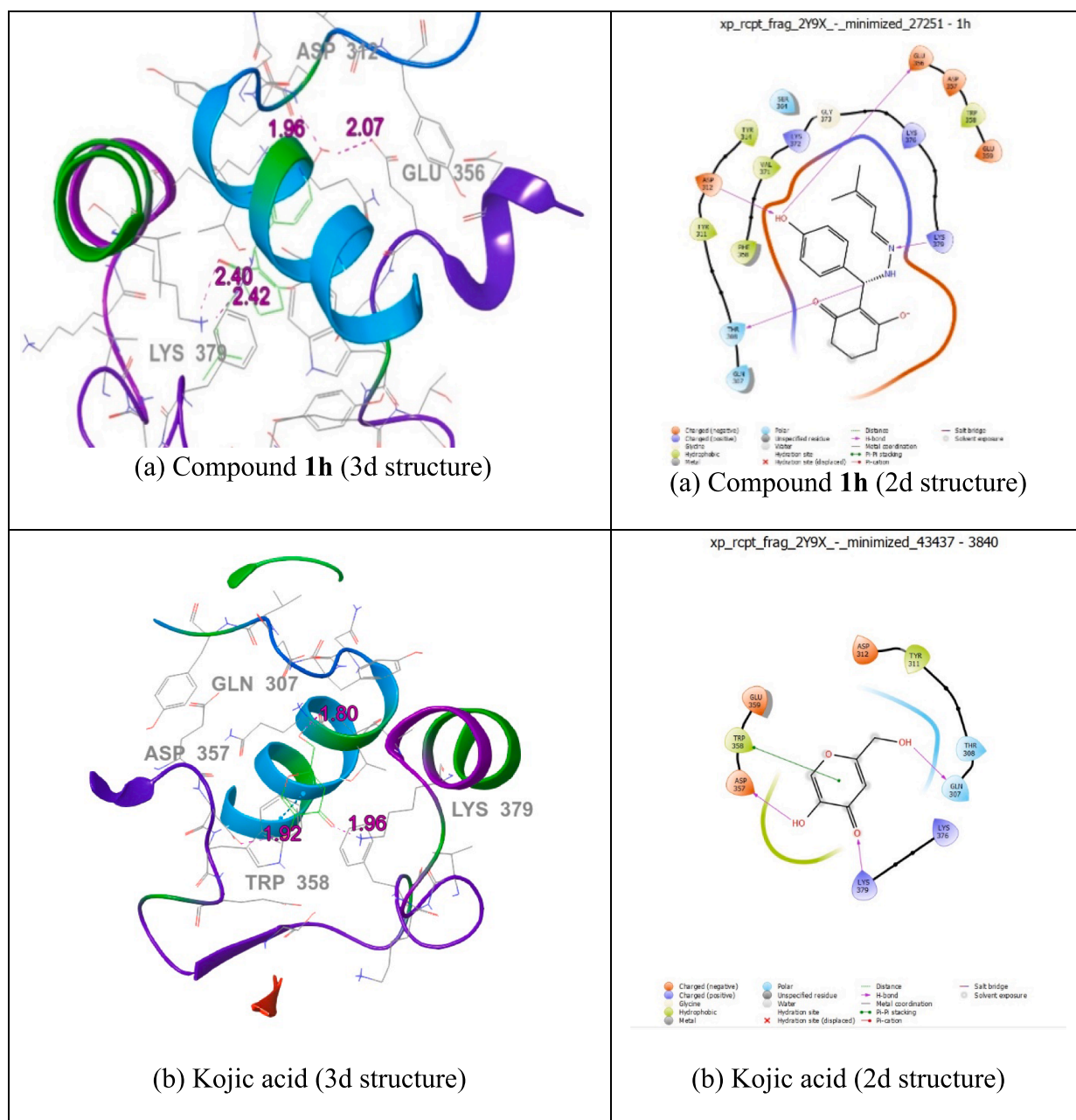#### 3.6.1. Molecular docking studies of anti-tyrosinase activity

Auto Dock Vina 1.1.2. program was used to evaluate the docking behaviour of compounds **1d, 1f, 1 h,** and kojic acid with mushroom

Table 5
Antibacterial screening for compounds **1a–1i.**

Compounds	*S. aureus*	*K. pneumonia*	*E. coli*	*P. aeruginosa*
1a	32	16	16	32
1b	4	16	8	8
1c	4	32	8	8
1d	2	0.5	2	1
1e	4	4	4	4
1f	2	16	8	4
1 g	8	16	4	2
1 h	4	16	16	2
1i	8	32	4	2
Ciprofloxacin	4	16	4	2

MIC (µg/mL) = Minimum inhibitory concentration

tyrosinase-binding protein (PDB ID: **2Y9X**). With the mushroom tyrosinase binding protein (PDB ID: **2Y9X**), compound **1 h** demonstrated a higher binding affinity (-4.3 kcal/mol) and bond length (1.96, 2.07, 2.40, and 2.42 Å) than kojic acid (-3.8 kcal/mol) and bond length (1.80, 1.92, 3.78, and 1.96 Å). Residues of the amino acids GLN 307, THR 308, TYR 311, ASP 312, TYR 314, GLU 356, ASP 357, TRP 358, GLU 359, SER 364, PHE 368, VAL 371, LYS 372, GLY 373, LYS 376, and LYS 379 were tangled into hydrophobic connections, as shown in Fig. 2(a). Docking of compound **1 h** is shown in Fig. 2(a). The lowest activity compound **1d** and **1f** has lower binding affinity (-3.5, and −2.9 kcal/mol) compared with Kojic acid and compound **1 h** compared. In the control kojic acid, the amino acid residues GLN307, THR308, TYR311, ASP312, ASP357, TRP358, GLU359, LYS376, and LYS379 were tangled in hydrophobic connections. The docking of the positive control kojic acid is shown in Fig. 2(b). The findings demonstrate that, in comparison to the controls, kojic acid and compounds **1d**, **1f**, and **1 h** have equivalent inhibitory capacities. The molecular docking results are presented in Table 6(a).

(a) Compound **1h** (3d structure)

(a) Compound **1h** (2d structure)

(b) Kojic acid (3d structure)

(b) Kojic acid (2d structure)

Fig. 2. Molecular docking studies of 2d and 3d structure of compound **1h** (a), **kojic acid** (b) with protein **2Y9X.**

Table 6

Molecular docking results of compound **1h**, **1d**, **1f**, kojic acid, and ciprofloxacin docked with protein **2Y9X** and **6B1P**.

(a) Compound **1h**, **1d**, **1f**, and **kojic acid** docked with protein **2Y9X**				
S. No	Compound name	Dock Score	Interacting residues	Bond Length
1	**1d**	−3.5	Asp 312, Lys 376, Lys 379(2)	2.13, 3.52, 2.58, 3.40
2	**1f**	−2.9	Asp 312, Lys 379	2.23, 4.10
3	**1 h**	−4.3	Asp 312, Glu 356, Lys 379(2)	1.96, 2.07, 2.40, 2.42
4	**kojic acid**	−3.8	Gln 307, Asp 357, Trp 358, Lys379	1.80, 1.92, 3.78, 1.96
(b) Compound **1h**, **1d**, **1f**, and ciprofloxacin docked with protein **6B1P**				
1	**1d**	−6.4	Arg 80, Arg 157	4.91, 2.55
2	**1f**	−5.5	Phe 141, Ala 153, Arg 157	4.97, 2.19, 2.44
3	**1h**	−5.8	Arg 80, Phe 128, Arg 157	4.72, 4.62, 2.15
4	**ciprofloxacin**	−6.3	Ile172, Arg175,Lys210	2.34, 2.27, 2.29, 2.74, 3.08

The docking results for other compounds are provided in the Supporting Information (Fig. S19).

3.6.2. Molecular docking studies of antibacterial activity

Auto Dock Vina 1.1.2. program was used to evaluate the docking behaviour of compounds 1d, 1f, 1 h, and ciprofloxacin with mushroom tyrosinase-binding protein (PDB ID: **6B1P**). With the Glutamate-tRNA Synthetase from Helicobacter pylori binding protein (PDB ID: **6B1P**), compound 1d demonstrated a higher binding affinity (-6.4 kcal/mol) and bond length (4.91, and 2.55 Å) than ciprofloxacin (-6.3 kcal/mol) and bond length (2.34, 2.27, 2.29, 2.74, and 3.08 Å). The residues GLU 44, ALA 45, TRP 46, ILE 47, ASN 79, ARG 80, ASP 81, PHE 82, LEU 83, VAL 132, ILE 137, GLN 138, PHE 141, ILE 152, ALA 153, MET 156, ARG 157, and SER 160 are tangled into hydrophobic connections, as shown in Fig. 3(a). Docking of compound 1d is shown in Fig. 3(a). The lowest activity compound 1f and 1h has lower binding affinity (-5.5, and −5.8 kcal/mol) compared with ciprofloxacin and compound 1d compared. In the ciprofloxacin control, the amino acid residues ILE172, ARG175, TYR182, ASN183, and LYS 210 were tangled in hydrophobic connections. The docking of the positive control, ciprofloxacin, is shown in

(a) Compound **1d** (3d structure)

(a) Compound **1d** (2d structure)

(b) Ciprofloxacin (3d structure)

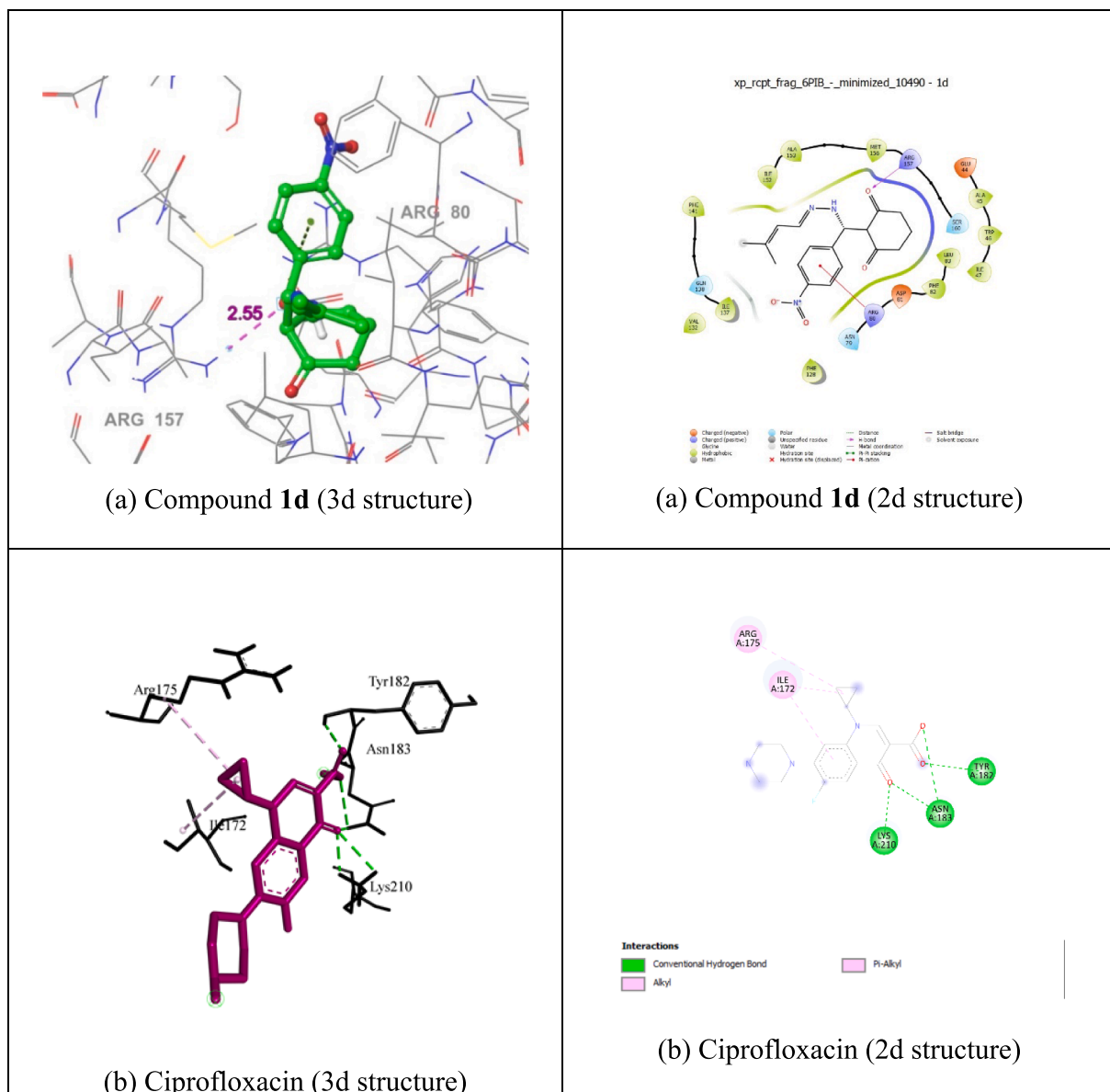(b) Ciprofloxacin (2d structure)

Fig. 3. Molecular docking studies of 2d and 3d structure of compound **1d** (a), and **ciprofloxacin** (b) with protein **6B1P**.

Fig. 3(b). These findings demonstrate that, in comparison to the controls, ciprofloxacin and compounds **1d, 1f,** and **1h** have equivalent inhibitory capacities. Molecular docking results are presented in Table 6 (b). The docking results for other compounds are provided in the Supporting Information (Fig. S20).

Finally, compounds **1h** and 2Y9X protein, docked in antityrosinase activity, produced a high docking score (−4.3 kcal/mol), and compounds **1d** and 6B1P protein, docked in antibacterial activity, produced a high docking score (−6.4 kcal/mol) (Akbar et al., 2022; Ali et al., 2020).

3.7. Structure–activity relationship (SAR) analysis

The chemical composition of molecules is biologically relevant to their biological activities in the test system, and this link is known as the structural-activity relationship (SAR). By investigating the relationships between structure and activity, we discovered many significant factors.

The SAR demonstrated a correlation between electrons and the presence of both drawing and electron-releasing groups at the C-4 position of the phenyl ring in relation to the hydrazine analogues **1a–i**. These compounds were found to be more potent against both gram-

positive and gram-negative microorganisms than ciprofloxacin. Compounds **1b** and **1h** displayed significant antibacterial activity against all bacterial species, with the SAR revealing the presence of strong electron-withdrawing groups ($-NO_2$) which indicated better antibacterial action. Additionally, the SAR showed that lipophilicity played a crucial role in antibacterial activity. While the substances **1d** (MIC = 0.5 μg/mL) was extremely active against *K. pneumoniae*, *Staphylococcus aureus*, and *Pseudomonas aeruginosa* (MIC = 1 μg/mL) had a highly activity compared to standard and other compounds (Al-Khattaf et al., 2021).

To evaluate the preliminary SARs, the cytotoxic activity results of the cimemoxin-Mannich base derivatives were utilised. The results of the selected Mannich base derivatives of cimemoxin (**1a-1i**) demonstrated that compound **1f** displayed the highest efficiency in controlling cancer cell proliferation ($IC_{50} = 0.12 \pm 0.04$ μg/mL) compared to doxorubicin. The presence of a cimemoxin ring along with a 4-methoxybenzaldehyde group resulted in enhanced cytotoxic activity against cancer cell lines. This was attributed to the electron-withdrawing methoxy group on the phenyl ring, which was attached to the cimemoxin skeleton. The other compounds displayed weak cytotoxic activity against all the tested cancer cell lines (Gobinath et al., 2021).

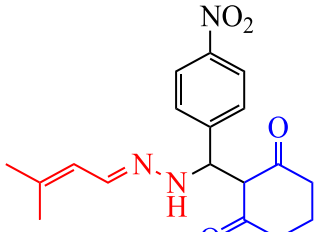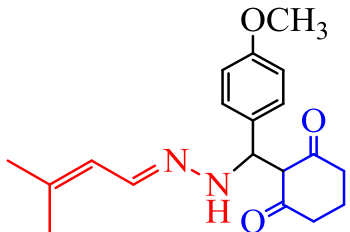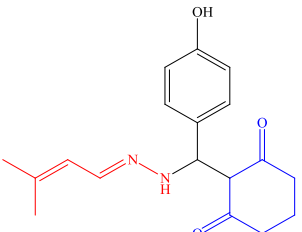Compound **1h** has (*E*)-(3-methylbut-2-en-1-ylidene)hydrazine,

1(d)		1(f)		1(h)	
Antioxidant activity					
DPPH: $IC_{50} = 76.48$ μg/mL		33.49 μg/mL		19.62 μg/mL	
H_2O_2: $IC_{50} = 47.42$ μg/mL		40.85 μg/mL		13.79 μg/mL	
NO: $IC_{50} = 48.00$ μg/mL		45.39 μg/mL		67.82 μg/mL	
ABTS•+: 80.32 ± 0.50 %		99.08 ± 0.02 %		92.32 ± 0.36 %	
AAPH: 80.24 ± 0.12 %		97.30 ± 0.10 %		92.01 ± 0.04 %	
Anti-tyrosinase activity					
$IC_{50} = 37.01$ μg/mL		43.88 μg/mL		15.16 μg/mL	
Cytotoxic activity					
$IC_{50} = 53.01 \pm 0.17$ μg/mL		0.12 ± 0.04 μg/mL		1.69 ± 0.05 μg/mL	
Antibacterial activity (μg/mL)					
S. aureus	*P. aeruginosa*	*S. aureus*	*P. aeruginosa*	*S. aureus*	*P. aeruginosa*
2	1	2	4	4	2

Fig. 4. Comparison of highly active compounds and the structure–activity relationship.

cyclohexane-1,3-dione, with an 4-nitrobenzaldehyde, demonstrating higher antioxidant activity (DPPH: IC$_{50}$ = 14.56 μg/mL, H$_2$O$_2$: IC$_{50}$ = 11.82 μg/mL) than compounds **1d** and **1f**. Compounds **1f** had high ABTS$^{•+}$ and AAPH activities (99.08 ± 0.02 % and 97.30 ± 0.10 %, respectively), and NO scavenging activity (NO: IC$_{50}$ = 10.36 μg/mL) compared with other compounds (Fig. 4).

Therefore, the development of new types of antioxidant and antibacterial drugs can benefit from the use of 4-methoxybenzaldehyde and (3-methylbut-2-en-1-ylidene) hydrazine linked with cyclohexane-1,3-dione.

4. Conclusion

The conversion method was used to create new cimemoxin derivative multicomponent compounds **(1a–i)** in high yields using a single-pot Mannich base that does not require catalysis. This procedure is economical, and yields reasonable results. In this study, the cytotoxic, antioxidant, and antibacterial activities of nine cimemoxin compounds were tested. Compounds 1h were very effective at scavenging DPPH and H$_2$O$_2$, and compound **1c** was very effective at scavenging NO. Compared to the Trolox standard, compound **1f** was much more active in the ABTS$^{•+}$ and AAPH tests. Compound **1h** (IC$_{50}$ = 15.16 μg/mL) was highly active against the standard BHT and other compounds. In comparison to regular kojic acid, compounds **1f** dramatically reduced cytotoxic activity, while compounds **1f** (GI$_{50}$ = 0.12 ± 0.04 μM) displayed highly active MCF-7 cancer cell line while no effect against normal Vero cancerous cells. Screening for in vitro antibacterial activity showed that compound **1d** was more active against *K. pneumoniae* than the standard ciprofloxacin and other compounds. In molecular docking, compounds **1h** and **2Y9X** protein, docked in antityrosinase activity, produced a high docking score (−4.3 kcal/mol), and compounds **1d** and **6B1P** protein, docked in antibacterial activity, produced a high docking score (−6.4 kcal/mol). Further study is required because lead compounds **1d** and **1h** constitute a new class of highly effective cytotoxic, antibacterial, and antioxidant agents.

Declaration of competing interest

The authors declare that they have no known competing financial interests or personal relationships that could have appeared to influence the work reported in this paper.

Acknowledgments

Appendix A. Supplementary material

Supplementary data to this article can be found online at https://doi.org/10.1016/j.jksus.2023.103011.

References

Aggarwal, R., Rani, C., Sadana, R., Busari, K., Sharma, C., Aneja, K.R., 2013. Chemistry & biology interface. Chem. Biol. 3 (6), 389–397.

Akbar, I., Radhakrishnan, S., Meenakshisundaram, K., Manilal, A., Hatamleh, A.A., Alnafisi, B.K., Balasubramani, R., 2022. Design of 1, 4-Dihydropyridine hybrid benzamide derivatives: synthesis and evaluation of analgesic activity and their molecular docking studies. Drug Des. Devel. Ther. 4021–4039. https://doi.org/10.2147/dddt.s357604.

Alaklabi, A., Arif, I.A., Ahamed, A., Kumar, R.S., Idhayadhulla, A., 2018. Evaluation of antioxidant and anticancer activities of chemical constituents of the Saururus chinensis root extracts. Saudi J. Biol. Sci. 25 (7), 1387–1392. https://doi.org/10.1016/j.sjbs.2016.12.021.

Ali, D., Alarifi, S., Chidambaram, S.K., Radhakrishnan, S.K., Akbar, I., 2020. Antimicrobial activity of novel 5-benzylidene-3-(3-phenylallylideneamino) imidazolidine-2, 4-dione derivatives causing clinical pathogens: synthesis and molecular docking studies. J. Infection Public Health 13 (12), 1951–1960. https://doi.org/10.1016/j.jiph.2020.09.017.

Al-Khattaf, F.S., Mani, A., Hatamleh, A.A., Akbar, I., 2021. Antimicrobial and cytotoxic activities of isoniazid connected menthone derivatives and their investigation of clinical pathogens causing infectious disease. J. Infect. Public Health 14 (4), 533–542. https://doi.org/10.1016/j.jiph.2020.12.033.

Al-Zharani, M., Al-Eissa, M.S., Rudayni, H.A., Ali, D., Alkahtani, S., Surendrakumar, R., Idhayadhulla, A., 2022. Pyrazolo [3, 4-b] pyridin-3 (2H)-one derivatives: synthesis and their investigation of mosquito larvicidal activity. J. King Saud Univ.-Sci. 34 (2), 101767 https://doi.org/10.1016/j.jksus.2021.101767.

Belghiti, M.E., Echihi, S., Dafali, A., Karzazi, Y., Bakasse, M., Elalaoui-Elabdallaoui, H., Tabyaoui, M., 2019. Computational simulation and statistical analysis on the relationship between corrosion inhibition efficiency and molecular structure of some hydrazine derivatives in phosphoric acid on mild steel surface. Appl. Surf. Sci. 491, 707–722. https://doi.org/10.1016/j.apsusc.2019.04.125.

Caine, B.A., Bronzato, M., Fraser, T., Kidley, N., Dardonville, C., Popelier, P.L., 2020. Aqueous pKa prediction for tautomerizable compounds using equilibrium bond lengths. Commun. Chem. 3 (1), 21. https://doi.org/10.1038/s42004-020-0264-7.

Caine, B. A., Bronzato, M., Fraser, T., Kidley, N., Dardonville, C., Popelier, P., 2019. Solving the Problem of Aqueous pKa Prediction for Tautomerizable Compounds Using Equilibrium Bond Lengths. https://doi.org/10.26434/chemrxiv.9766907.

Chen, J., Hu, L., Hu, G., Zhang, Y., Hu, Y., Song, J., 2016. An application of chemical oscillation: distinguishing two isomers between cyclohexane-1, 3-dione and 1, 4-cyclohexanedione. Electrochimica Acta 195, 223–229. https://doi.org/10.1016/j.electacta.2016.02.141.

Chidambaram, S., Ali, D., Alarifi, S., Gurusamy, R., Radhakrishnan, S., Akbar, I., 2021. Tyrosinase-mediated synthesis of larvicidal active 1, 5-diphenyl pent-4-en-1-one derivatives against Culex quinquefasciatus and investigation of their ichthyotoxicity. Sci. Rep. 11 (1), 20730. https://doi.org/10.1038/s41598-021-98281-5.

El Azzouzi, M., Aouniti, A., Tighadouin, S., Elmsellem, H., Radi, S., Hammouti, B., Zarrouk, A., 2016. Some hydrazine derivatives as corrosion inhibitors for mild steel in 1.0 M HCl: weight loss, electrochemichal, SEM and theoretical studies. J. Mol. Liq. 221, 633–641. https://doi.org/10.1016/j.molliq.2016.06.007.

Etter, M.C., Urbanczyk-Lipkowska, Z., Jahn, D.A., 1986. Solid-state structural characterization of 1, 3-cyclohexanedione and of a 6: 1 cyclohexanedione-benzene cyclamer complex, a novel host-guest species. J. Am. Chem. Soc. 108 (19), 5871–5876. https://doi.org/10.1021/ja00279a035.

Ghosh, A., Tiwari, G.J., 2018. Role of nitric oxide-scavenging activity of Karanjin and Pongapin in the treatment of Psoriasis. 3 Biotech 8 (8), 338. https://doi.org/10.1007/s13205-018-1337-5.

Gobinath, P., Packialakshmi, P., Vijayakumar, K., Abdellattif, M.H., Shahbaaz, M., Idhayadhulla, A., Surendrakumar, R., 2021. Synthesis and cytotoxic activity of novel indole derivatives and their in silico screening on spike glycoprotein of SARS-CoV- 2. Front. Mol. Biosci. 8 https://doi.org/10.3389/fmolb.2021.637989.

Gong, J., Sumathy, K., Qiao, Q., Zhou, Z., 2017. Review on dye-sensitized solar cells (DSSCs): advanced techniques and research trends. Renew. Sustain. Energy Rev. 68, 234–246. https://doi.org/10.1016/j.rser.2016.09.097.

Hou, Y., Xu, L., Wei, Z., Liu, Y., Li, X., Deng, S., 2014. Reaction process and kinetics of the selective hydrogenation of resorcinol into 1, 3-cyclohexanedione. J. Taiwan Institute Chem. Eng. 45 (4), 1428–1434. https://doi.org/10.1016/j.jtice.2013.12.007.

Jung, Y., Ju, I.G., Choe, Y.H., Kim, Y., Park, S., Hyun, Y.M., Kim, D., 2019. Hydrazine exposé: the next-generation fluorescent probe. ACS Sensors 4 (2), 441–449. https://doi.org/10.1021/acssensors.8b01429.

Lateef, A., Ojo, S.A., Elegbede, J.A., Azeez, M.A., Yekeen, T.A., Akinboro, A., 2017. Evaluation of some biosynthesized silver nanoparticles for biomedical applications: hydrogen peroxide scavenging, anticoagulant and thrombolytic activities. J. Clust. Sci. 28, 1379–1392. https://doi.org/10.1007/s10876-016-1146-0.

Mani, A., Ahamed, A., Ali, D., Alarifi, S., Akbar, I., 2021. Dopamine-mediated vanillin multicomponent derivative synthesis via grindstone method: application of antioxidant, anti-tyrosinase, and cytotoxic activities. Drug Des. Devel. Ther. 787–802. https://doi.org/10.2147/dddt.s288389.

Markova, N.V., Rogojerov, M.I., Angelova, V.T., Vassilev, N.G., 2019. Experimental and theoretical conformational studies of hydrazine derivatives bearing a chromene scaffold. J. Mol. Struct. 1198, 126880 https://doi.org/10.1016/j.molstruc.2019.126880.

Mostafa, A.A.F., SathishKumar, C., Al-Askar, A.A., Sayed, S.R., SurendraKumar, R., Idhayadhulla, A., 2019. Synthesis of novel benzopyran-connected pyrimidine and pyrazole derivatives via a green method using Cu (II)-tyrosinase enzyme catalyst as potential larvicidal, antifeedant activities. RSC Adv. 9 (44), 25533–25543. https://doi.org/10.1039/C9RA04496E.

Pan, X., Chen, L., Xu, W., Bao, S., Wang, J., Cui, X., Chen, R., 2021. Activation of monoaminergic system contributes to the antidepressant-and anxiolytic-like effects of J147. Behav. Brain Res. 411, 113374 https://doi.org/10.1016/j.bbr.2021.113374.

Popiołek, Ł., 2017. Hydrazide–hydrazones as potential antimicrobial agents: overview of the literature since 2010. Med. Chem. Res. 26, 287–301. https://doi.org/10.1007/s00044-016-1756-y.

Selvaraj, K., Daoud, A., Alarifi, S., Idhayadhulla, A., 2020. Tel-Cu-NPs catalyst: Synthesis of naphtho [2, 3-g] phthalazine derivatives as potential inhibiters of tyrosinase enzymes and their investigation in kinetic, molecular docking, and cytotoxicity studies. Catalysts 10 (12), 1442. https://doi.org/10.3390/catal10121442.

Sharma, D., Kumar, M., Das, P., 2021. Synthetic approaches for cyclohexane-1, 3-diones: a versatile precursor for bioactive molecules. Synth. Commun. 51 (17), 2553–2573. https://doi.org/10.1080/00397911.2021.1946824.

Sun, H., Deng, J., Qiu, L., Fang, X., Peng, H., 2015. Recent progress in solar cells based on one-dimensional nanomaterials. Energ. Environ. Sci. 8 (4), 1139–1159. https://doi.org/10.1039/C4EE03853C.

Surendra Kumar, R., Moydeen, M., Al-Deyab, S., Manilal, A., Idhayadhulla, A., 2017. Synthesis of new morpholine-connected pyrazolidine derivatives and their antimicrobial, antioxidant, and cytotoxic activities. Bioorg. Med. Chem. Lett. 27, 66–71. https://doi.org/10.1016/j.bmcl.2016.11.032.

Tanini, D., Capperucci, A., 2021. Synthesis and applications of organic selenols. Adv. Synth. Catal. 363 (24), 5360–5385. https://doi.org/10.1002/adsc.202101147.

Wei, Z., Liu, H., Chen, Y., Guo, D., Pan, R., Liu, Y., 2018. Mechanistic insights into the selective hydrogenation of resorcinol to 1, 3-cyclohexanedione over Pd/rGO catalyst through DFT calculation. https://doi.org/10.1016/j.cjche.2018.01.031.